Chapter 5

On the Fluid-Structure Interaction of a Composite Wind Turbine Blade

Roham Rafiee

Composites Research Laboratory, Faculty of New Sciences & Technologies,
University of Tehran, Tehran, 1439955941, Iran

Roham.Rafiee@ut.ac.ir

I. INTRODUCTION

Global warming of the earth and lack of fossil fuels from one hand and the increasing demand for electricity from other hand have turned the global attentions toward pollution free electricity generation from clean and renewable energy resources. Among different renewable energy resources, wind energy is of growing importance which can be inferred from the installed capacity of the wind turbines during the past decades. As a frontier element in capturing wind energy, the blade plays a key role in the efficient performance of a wind turbine dictated by economical power generation indicators. The importance of blade is a twofold issue: it is required not only to get as much wind energy as possible in a limited period of time that wind flows; but also to present a structure capable of operating for about 20 years without any severe defect. Consequently, the wind turbine blade has to incorporate both proper aerodynamic performance and appropriate structural stiffness at the same time exposing to different working conditions.

A wind turbine blade is required to provide a strong and light structure in order to accommodate different loading conditions during different experienced events by the wind turbine and also start operating at low wind speed regime. These should be accomplished while the aerodynamic performance is maintained in optimum condition during the lifetime. Moreover, random nature of wind flow, long and flexible structure of wind turbine blades and their continuous operation under different circumstances render them as fatigue critical components. From structural point of view, the composite materials are the only solution addressing all aforementioned structural design constraints. The blades of the modern horizontal axis wind turbines (HAWT) are full composite structures which are generally made of Glass/Epoxy while in a very long blade a hybrid configuration of Carbon/Epoxy and Glass/Epoxy in critical areas is used [1]. Fig. 1 shows a production process of a 23-meter composite wind turbine blade using hand lay-up process utilizing Prepreg materials while the longer wind turbine blades are manufactured using vacuum infusion process (VIP) method for better and more uniform impregnation of dry fabrics and more rapid mass production [2].

Fig. 1 A production process of a composite wind turbine blade using hand lay-up method (Courtesy of Sabaniroo Co., Iran)

Converting kinematic energy of wind inflow to electricity, the generated power by wind turbines is proportional to the swept area by the rotor [3]. Thus, it would be reasonable to increase the cost efficiency of a wind turbine by increasing the rotor diameter. Nowadays, the modern HAWTs with the capacity of 500 kW up to 5 MW are equipped with the blade length ranging from 15 to 75 meters. An increasing trend in the length of a wind turbine blade demands more clarified understanding

of its structural behaviour from different viewpoints. The investigation of the interaction between aerodynamics and structure which falls into aeroelasticity study has to be taken into account during the design process of wind turbine. The lack of control regarding this interaction may lead to a reduction in power production capability of a wind turbine. A wind turbine blade is subjected to aerodynamic loadings which will induce some variations to the primary geometry of the blade. The variation in the geometrical shape is not negligible due to the flexible structure of blades; and this will, however, cause some variations in imposed aerodynamic forces. Increasing the level of the blade deflection engenders significant changes in the elastic and aerodynamics forces, thus affecting the overall performance of a wind turbine. This phenomenon will also cause some uncertainties in induced stress components in the critical region of the blade.

II. STATE OF THE ART

The main objective of this chapter is (i) to study the fluid-structure interaction on a commercial wind turbine blade under various operational conditions and (ii) to evaluate the degree to which this phenomenon will change the stress components in composite layers of the investigated blade structure. A semi-coupled method as an iterative approach is employed in this context to perform aeroelastic analysis on a specific wind turbine blade. A semi-coupled technique implies on dividing the problem into fluid and structural spaces which are solved sequentially and the output of each space is fed into the other space as input.

The wind turbine blade under consideration in this study belongs to 660 kW wind turbine, manufactured in Iran after technology transfer from Vestas Wind System A/S [4]. The rotor of the investigated wind turbine consists of three blades and a nose cone. The rotor drives the main shaft of the wind turbine which is connected to the three-stage planetary gearbox with 1:52 ratio. The output of the gearbox is transmitted to an asynchronized generator which produces 660 kW electricity. The whole components for transmitting kinematic energy of the wind flow and power generation are placed inside the nacelle on the top of 42 meter tower. Installed in Iran, the whole wind turbine structure is shown in Fig. 2. The investigated wind turbine is categorized under the constant speed type by maintaining the rotating speed of rotor at 28.5 rpm using pitch power regulation system. The power regulating mechanism makes blades rotate about 89 degree along their longitudinal axis dependently. Thus, the angle of attack in different cross sections of a blade is changed in accordance with wind speed variation. Moreover the wind turbine is equipped with active yaw control system keeping turbine in wind flow direction by rotating the whole nacelle around the tower.

Fig. 2 Investigated 660 kW wind turbine (Courtesy of Sabaniroo Co., Iran)

The length of the blade investigated within this chapter is 23 meters and its mass is about 1250 kg. The structure of the blade consists of two main structural parts (shell and spar). The spar is located inside the shell, it is mainly responsible to support different load cases and its cross section has a box shape. The shell of the blade provides pressure distribution required for blade rotation and thus its cross section is in the form of specific airfoils due to aerodynamic considerations associated with efficiency of the blade in capturing wind energy. It can be understood that while the spar contributes considerably to the structural aspects of the blade, the shell is responsible for aerodynamic performance of the blade. This wind turbine blade has a twist angle about 15 degrees from root to tip to keep the angles of attack all along the blade compatible with relative wind velocity and the blade has also a tapered shape.

III. MODELLING

Model preparation includes constructing geometrical and finite element models for both aerodynamic and structural analyses. Firstly, a fundamental geometrical model of the blade is constructed as a wireframe model on the basis of available cross section profiles of the shell and spar in different stations from the root to the tip of the blade. The Loft method is used to draw surface in the spaces between these cross sections converting the wireframe to surface model. Both wireframe and surface models are shown in Fig. 3.

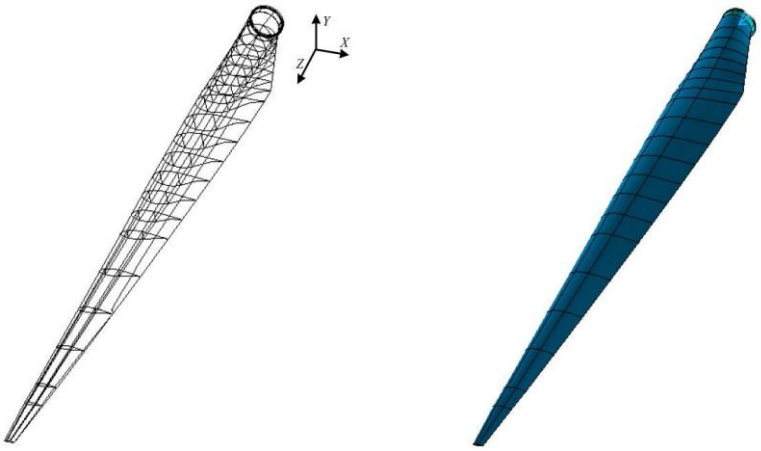

Fig. 3 Wireframe (left) and surface (right) models of the wind turbine blade

For constructing structural finite element model, second order shell elements were selected from element library of ANSYS [5]. The selected element is powered with a feature to analyse layered shells which is compatible with composite plies of the structure. Thanks to manual meshing method, the whole model contains quadratic elements with appropriate aspect ratio avoiding any triangular element. From structural convergence study on the mesh density of the model, it is inferred that 8505 elements are sufficient for the finite element analysis. The whole nodes placed on the root region of the model are restricted from any movement as the boundary conditions used in the case of static analysis. The procedure of obtaining mechanical properties of composite layers is comprehensively explained in the next section.

The aerodynamic finite element model is constructed on the same geometry platform used for structural analysis. Following the same pattern of the blade outer elements, fluid elements which are in direct contact with blade surface are constructed using FLOTRAN142 and free mesh method [5]. Wind velocity along X-direction on the side planes are constantly taken as free wind flow speed. Multiplying angular velocity of the blade by the radius of blade at each station, the linear velocity of the blade due to rotation is obtained and applied to each corresponding station in Y-direction. The applied pressure on the trailing edge of the wind blade is taken equal to zero. Due to no-slip condition, velocity is taken equal to zero in all directions on the shell.

IV. MATERIAL PROPERTIES

Three different types of Prepreg Glass/Epoxy fabrics are used in the manufacture of structural blades. Tri-axial and bi-axial fabrics are used in the shell structure in the form of [0/±45] and [±45], respectively. Bi-axial and Uni-directional (U-D) fabrics are used in the spar structure. It is worth mentioning that tri-axial and bi-axial fabrics utilized for manufacturing the investigated wind turbine blade are not woven fabrics and U-D plies with mentioned orientations are stitched together. Two kinds of foams are also used in the shell and spar structure to provide sandwich panels. Prepregs have had a considerable impact on the evolution of composite industries in the late 20th century. Used in all aerospace programs worldwide, they are also enabling a new generation of high speed trains and fast ships and long wind turbine blades to become reality rather than designer's dream. A Prepreg consists of a combination of a matrix (e.g., resin) and fibre reinforcement. It is ready to use in the component manufacturing process. In this technology, reinforcing fibres are impregnated with resin before manufacturing process and this makes the process easier and more economic [6]. Furthermore, control of fibre volume fraction is handled better. The fabrics consist of at least two threads that are weaved together and called "warp" and "weft" or are stitched together in non-woven form. The weave style can be varied according to crimp and drapeability. Low crimp gives better mechanical performance because straighter fabrics carry greater loads [6]. It has been proven that crimp will negatively affect fatigue life of structure [7]. Geometric of woven fabric produces out of plane curvature in plies and consequently stress concentration appears. Compressive strength of fibres in woven fabrics is approximately half of straight fibres in stitched form [8]. In order to overcome this problem using stitched form instead of woven fabrics is recommended [8]. The main criteria that influence the selection of Prepregs for particular application are performance and cost and the main advantages of using them can be summarized as lower fabrication cost, reduced energy consumption, optimized weight and better mechanical properties under cyclic loading, tensile, stiffness and corrosion.

For structural FE analysis, complete sets of mechanical properties are required. Mechanical properties of U-D are available experimentally, while limited data are available for bi-axial and tri-axial laminates. Namely, elastic moduli in 0° and 45° directions are experimentally available for these laminates [9] as depicted in Fig. 4. Bi-axial and tri-axial laminates can be both taken into account sometimes as [±45] and [0/±45] when 0° in Fig. 4 is considered and sometimes they can be considered as [0/90] and [0/90/-45], respectively, when 45° direction in Fig. 4 is considered. The available and non-available mechanical properties of all aforementioned layers are presented in Table 1.

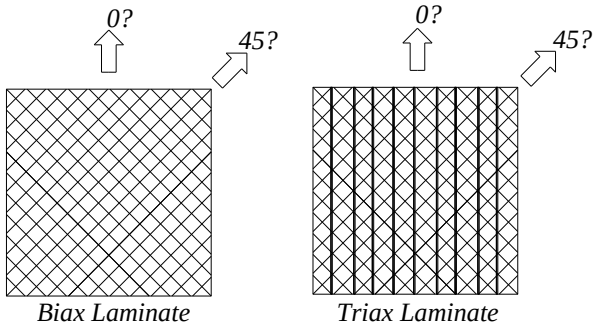

Fig. 4 Directions of Bi-axial and Tri-axial Laminates

As it can be seen from Table 1, elastic moduli E_1 and E_2 are equal in [±45], [0/90] and [0/90/-45] due to symmetry. Since both tri-axial and bi-axial laminates consist of the same U-D fibres stitched together, the non-available properties of these laminates can be obtained.

TABLE 1 AVAILABLE AND NOT-AVAILABLE MECHANICAL PROPERTIES [9]

Laminate Name	Configuration	E_1 (GPa)	E_2 (GPa)	ν_{12}	E_6 (GPa)
U-D	[0]	43	9.77	0.32	3.31
Bi-axial	[±45]	6.8	6.8	N/A	N/A
Bi-axial	[0/90]	16.7	16.7	N/A	N/A
Tri-axial	[0/±45]	20.7±3.1	N/A	N/A	N/A
Tri-axial	[0/90/-45]	15.1±2.3	15.1±2.3	N/A	N/A

A. General governing equations

Stiffness matrix of a U-D ply is written as [10]:

$$\begin{bmatrix} Q_{XX} & Q_{XY} & 0 \\ Q_{XY} & Q_{YY} & 0 \\ 0 & 0 & Q_{SS} \end{bmatrix} \tag{1}$$

where,

$$Q_{XX} = \frac{E_X}{1-\nu_{XY}\nu_{YX}} \quad , \quad Q_{YY} = \frac{E_Y}{1-\nu_{XY}\nu_{YX}} \quad , \quad Q_{XY} = \frac{\nu_{YX}E_X}{1-\nu_{XY}\nu_{YX}} \quad , \quad Q_{SS} = G \tag{2}$$

Involved parameters in set of Eq. (2) are in the space of on-axis coordinate system and "*x*" devotes to longitudinal fibre direction and "*y*" devoted to transverse direction. ν_{XY} is major Poisson's ratio and ν_{YX} is minor Poisson's ratio. If one needs stiffness matrix in any desired direction, transformation from on-axis coordinate system to off-axis has to be performed using following relation [11]:

$$\begin{bmatrix} Q_{11} \\ Q_{22} \\ Q_{12} \\ Q_{66} \\ Q_{16} \\ Q_{26} \end{bmatrix} = \begin{bmatrix} m^4 & n^4 & 2m^2n^2 & 4m^2n^2 \\ n^4 & m^4 & 2m^2n^2 & 4m^2n^2 \\ m^2n^2 & m^2n^2 & m^4+n^4 & -4m^2n^2 \\ m^2n^2 & m^2n^2 & -2m^2n^2 & (m^2-n^2)^2 \\ m^3n & -mn^3 & mn^3-m^3n & 2(mn^3-m^3n) \\ mn^3 & -m^3n & mn^3-m^3n & 2(mn^3-m^3n) \end{bmatrix} \begin{bmatrix} Q_{XX} \\ Q_{YY} \\ Q_{XY} \\ Q_{SS} \end{bmatrix} \tag{3}$$

$$m = Cos\theta \quad , \quad n = Sin\theta$$

For the ply where fibres are oriented in the direction of 0 °, we have:

$$\begin{aligned} Q^0_{11} &= Q_{XX} \\ Q^0_{22} &= Q_{YY} \\ Q^0_{12} &= Q^0_{21} = Q_{XY} \\ Q^0_{66} &= Q_{SS} \\ Q^0_{16} &= Q^0_{26} = 0 \end{aligned} \tag{4}$$

Similarity, for ply with fibres at 90 °:

$$\begin{aligned} Q_{11}^{90} &= Q_{22}^{0} \\ Q_{22}^{90} &= Q_{11}^{0} \\ Q_{12}^{90} &= Q_{21}^{90} = Q_{12}^{0} \\ Q_{66}^{90} &= Q_{66}^{0} \\ Q_{16}^{90} &= Q_{26}^{90} = Q_{16}^{0} \end{aligned} \tag{5}$$

For a 45 °ply and a -45 °ply, we have:

$$\begin{aligned} Q_{11}^{45} &= Q_{11}^{-45} \\ Q_{22}^{45} &= Q_{22}^{-45} \\ Q_{12}^{45} &= Q_{21}^{45} = Q_{12}^{-45} = Q_{21}^{-45} \\ Q_{66}^{45} &= Q_{66}^{-45} \\ Q_{16}^{45} &= Q_{26}^{45} = -Q_{16}^{-45} = -Q_{26}^{-45} \end{aligned} \tag{6}$$

Equivalent stiffness matrix of a composite composed of two plies can be calculated using the following relation:

$$\frac{1}{h}A_{ij} = Q_{ij}^{\alpha}p^{\alpha} + Q_{ij}^{\beta}p^{\beta} \tag{7}$$

where, "*h*" is the laminate thickness, α is the angle of first ply in accordance of selected coordinate system, β is the angle of second ply and "*p*" is the ply fraction. Based on technical data from supplier of investigated bi-axial laminate [9], both ply fractions are considered to be the same. Therefore, we have:

$$p^{0} = p^{90} = p^{45} = p^{-45} = 0.5 \tag{8}$$

Using Eqs. (7) and (8), we have:

$$\frac{1}{h}A_{ij}^{[0/90]} = 0.5(Q_{ij}^{0} + Q_{ij}^{90}) \qquad \frac{1}{h}A_{ij}^{[45/-45]} = 0.5(Q_{ij}^{45} + Q_{ij}^{-45}) \tag{9}$$

By calculating the inverse of matrix [*A*], we have:

$$\left[\frac{1}{h}[A]\right]^{-1} = h[A]^{-1} = h[a] \tag{10}$$

Where, [*a*] is the compliance matrix and its terms are as follows [11]:

$$[a] = h\begin{bmatrix} 1/E_1 & -\nu_{12}/E_2 & \nu_{16}/E_6 \\ -\nu_{12}/E_2 & 1/E_2 & \nu_{26}/E_6 \\ \nu_{16}/E_6 & \nu_{26}/E_6 & 1/E_6 \end{bmatrix} \tag{11}$$

It can be seen that in Eq. (11), all "*x*" and "*y*" superscripts have been changed to numerical superscripts which representing properties of a laminated composite instead of single ply. Now, the same calculation has to be performed for other aforementioned configurations.

B. Bi-axial Laminate with [±45] Configuration

Stiffness matrix of this composite is calculated using Eqs. (3), (6) and (9):

$$\frac{1}{h}[A^{[\pm 45]}] = \frac{1}{h}\begin{bmatrix} A_{11}^{[\pm 45]} & A_{11}^{[\pm 45]} & 0 \\ A_{11}^{[\pm 45]} & A_{11}^{[\pm 45]} & 0 \\ 0 & 0 & A_{11}^{[\pm 45]} \end{bmatrix}$$

$$\begin{aligned} [A_{11}^{[\pm 45]}] &= 0.25Q_{XX} + 0.5Q_{XY} + 0.25Q_{YY} + Q_{SS} \\ [A_{22}^{[\pm 45]}] &= 0.25Q_{XX} + 0.5Q_{XY} + 0.25Q_{YY} + Q_{SS} \\ [A_{12}^{[\pm 45]}] &= [A_{21}^{[\pm 45]}] = 0.25Q_{XX} + 0.5Q_{XY} + 0.25Q_{YY} - Q_{SS} \\ [A_{66}^{[\pm 45]}] &= 0.25Q_{XX} - 0.5Q_{XY} + 0.25Q_{YY} \end{aligned} \tag{12}$$

Compliance matrix is calculated using Eq. (11), after replacing known parameters by their values given in Table 1:

$$[a] = h\begin{bmatrix} 1/6.8 & -\alpha/6.8 & 0 \\ -\alpha/6.8 & 1/6.8 & 0 \\ 0 & 0 & 1/G_{[\pm 45]} \end{bmatrix} \tag{13}$$

where, α is the major Poisson's ratio of bi-axial laminates.

After inversing matrix [*a*] expressed by Eq. (13), equalizing them to their corresponding members in Eq. (12) and omitting repeated equations, we get:

$$\begin{aligned} 0.25Q_{XX} + 0.5Q_{XY} + 0.25Q_{YY} + Q_{SS} &= \frac{0.147059}{0.0216263 - 0.0216263\alpha^2} \\ 0.25Q_{XX} + 0.5Q_{XY} + 0.25Q_{YY} - Q_{SS} &= \frac{0.147059\alpha}{0.0216263 - 0.0216263\alpha^2} \\ 0.25Q_{XX} - 0.5Q_{XY} + 0.25Q_{YY} &= G_{[\pm 45]} \end{aligned} \tag{14}$$

C. Bi-axial Laminates with [0/90] Configuration

Stiffness matrix of this configuration is derived using Eqs. (3), (5) and (9):

$$\frac{1}{h}[A^{0/90}] = \frac{1}{h}\begin{bmatrix} 0.5Q_{XX} + 0.5Q_{YY} & Q_{XY} & 0 \\ Q_{XY} & 0.5Q_{XX} + 0.5Q_{YY} & 0 \\ 0 & 0 & Q_{SS} \end{bmatrix} \tag{15}$$

Compliance matrix is calculated using Eq. (11), after replacing known parameters by their values given in Table 1:

$$[a] = h\begin{bmatrix} 1/16.7 & -\beta/16.7 & 0 \\ -\beta/16.7 & 1/16.7 & 0 \\ 0 & 0 & 1/G_{[0/90]} \end{bmatrix} \tag{16}$$

where, β is major Poisson's ratio of composites.

After inversing the matrix expressed by Eq. (16), equalizing them to their corresponding members in Eq. (15) and omitting repeated equations, we have:

$$\begin{aligned} 0.5Q_{XX} + 0.5Q_{YY} &= \frac{0.0598802}{0.00358564 - 0.00358564\beta^2} \\ Q_{XY} &= \frac{0.0598802\beta}{0.00358564 - 0.00358564\beta^2} \\ Q_{SS} &= G_{[0/90]} \end{aligned} \tag{17}$$

D. Tri-axial Laminate with [0/±45] Configuration

In order to calculate matrices related to tri-axial composites, the same method of bi-axial laminate is employed. The only difference is referred to ply fractions. According to information from supplier [9], the amount of fibres in 0 °direction is equal to 254 kg/m^2 and the amount of fibres in 45 °direction and -45 °direction is equal to 230 kg/m^2. Therefore, we have:

$$\begin{aligned} p^0 &= \frac{425}{425 + 230 + 230} = 0.48 \\ p^{45} = p^{-45} &= \frac{230}{425 + 230 + 230} = 0.26 \end{aligned} \tag{18}$$

Stiffness matrix of this configuration is can be written in the following form using Eqs. (4), (6), (7) and (18):

$$\frac{1}{h}[A^{[0/\pm 45]}] = \frac{1}{h}\begin{bmatrix} 0.61Q_{XX} + 0.26Q_{XY} + 0.13Q_{YY} + 0.52Q_{SS} & 0.13Q_{XX} + 0.74Q_{XY} + 0.13Q_{YY} - 0.52Q_{SS} & 0 \\ 0.13Q_{XX} + 0.74Q_{XY} + 0.13Q_{YY} - 0.52Q_{SS} & 0.13Q_{XX} + 0.26Q_{XY} + 0.61Q_{YY} + 0.52Q_{SS} & 0 \\ 0 & 0 & 0.13Q_{XX} - 0.26Q_{XY} + 0.13Q_{YY} + 0.48Q_{SS} \end{bmatrix} \tag{19}$$

Compliance matrix is calculated using Eq. (11) and known parameters given in Table 1:

$$[a]=h\begin{bmatrix} 1/(20.7\pm3.1) & -\varphi/(20.7\pm3.1) & 0 \\ -\varphi/(20.7\pm3.1) & 1/E_2 & 0 \\ 0 & 0 & 1/G_{[0/\pm45]} \end{bmatrix} \tag{20}$$

Where, φ is the major Poisson's ratio of the tri-axial composites with [0/±45] configuration.

After inversing the matrix expressed by Eq. (20), equalizing them to their corresponding members in Eq. (19) and omitting repeated equations, we have:

$$\begin{aligned} 0.61Q_{XX}+0.26Q_{XY}+0.13Q_{YY}+0.52Q_{SS} &= \frac{1}{0.0483092-0.00233378E_2\varphi^2} \\ 0.13Q_{XX}+0.26Q_{XY}+0.61Q_{YY}+0.52Q_{SS} &= \frac{0.0483092E_2}{0.0483092-0.00233378E_2\varphi^2} \\ 0.13Q_{XX}+0.74Q_{XY}+0.13Q_{YY}-0.52Q_{SS} &= \frac{0.0483092E_2\varphi}{0.0483092-0.00233378E_2\varphi^2} \\ 0.13Q_{XX}-0.26Q_{XY}+0.13Q_{YY}+0.48Q_{SS} &= G_{[0/\pm45]} \end{aligned} \tag{21}$$

E. Tri-axial Laminate with [0/90/-45] Configuration

Extraction method of stiffness matrix of this configuration is the same as the method employed for the case of tri-axial laminates with [0/±45] configuration. The only difference can be found in ply fraction due to new distribution of fibres as below:

$$\begin{aligned} p^{-45} &= \frac{425}{425+230+230}=0.48 \\ p^{0}=p^{90} &= \frac{230}{425+230+230}=0.26 \end{aligned} \tag{22}$$

Stiffness matrix of this configuration can be written in the following form using Eqs. (4)- (7) and (22):

$$\frac{1}{h}[A^{[0/90/-45]}]=\frac{1}{h}\begin{bmatrix} 0.38Q_{XX}+0.24Q_{XY}+0.38Q_{YY}+0.48Q_{SS} & 0.12Q_{XX}+0.76Q_{XY}+0.12Q_{YY}-0.48Q_{SS} & -0.12Q_{xx}+0.12Q_{YY} \\ 0.12Q_{XX}+0.76Q_{XY}+0.12Q_{YY}-0.48Q_{SS} & 0.38Q_{XX}+0.24Q_{XY}+0.38Q_{YY}+0.48Q_{SS} & -0.12Q_{xx}+0.12Q_{YY} \\ -0.12Q_{xx}+0.12Q_{YY} & -0.12Q_{xx}+0.12Q_{YY} & 0.12Q_{XX}-0.24Q_{XY}+0.12Q_{YY}+0.52Q_{SS} \end{bmatrix} \tag{23}$$

Compliance matrix is calculated using Eq. (11) and the known parameters given in Table 1:

$$[a]=h\begin{bmatrix} 1/(15\pm2.3) & -\xi/(15\pm2.3) & \mu/G_{[0/90/-45]} \\ -\xi/(15\pm2.3) & 1/(15\pm2.3) & \mu/G_{[0/90/-45]} \\ \mu/G_{[0/90/-45]} & \mu/G_{[0/90/-45]} & 1/G_{[0/90/-45]} \end{bmatrix} \tag{24}$$

where, ξ is the minor Poisson's ratio of tri-axial laminate with [0/90/-45] configuration and μ is the coupling Poisson's ratio in "16" plan. In general case, Q_{16} is not equal to Q_{26}. But in this particular case, it can be seen that these two parameters are equal and it has to be considered in compliance matrix too.

After inversing the matrix expressed by Eq. (24), equalizing them to their corresponding members in Eq. (23) and omitting repeated equations, we have:

$$
\begin{aligned}
0.38Q_{XX} + 0.24Q_{XY} + 0.38Q_{YY} + 0.48Q_{SS} &= \frac{0.066G_{[0/90/-45]} - \eta^2}{G_{[0/90/-45]}(0.004356 - 0.004356\xi^2) - 0.132(1+\xi)\eta^2} \\
0.12Q_{XX} + 0.76Q_{XY} + 0.12Q_{YY} - 0.48Q_{SS} &= \frac{0.066G_{[0/90/-45]} + \eta^2}{G_{[0/90/-45]}(0.004356 - 0.004356\xi^2) - 0.132(1+\xi)\eta^2} \\
0.13Q_{XX} + 0.74Q_{XY} + 0.13Q_{YY} - 0.52Q_{SS} &= \frac{0.066G_{[0/90/-45]}(1+\xi)\eta}{G_{[0/90/-45]}(0.004356 - 0.004356\xi^2) - 0.132(1+\xi)\eta^2} \\
0.12Q_{XX} - 0.24Q_{XY} + 0.12Q_{YY} + 0.52Q_{SS} &= \frac{G^2_{[0/90/-45]}(0.004356 - 0.004356\xi^2)}{G_{[0/90/-45]}(0.004356 - 0.004356\xi^2) - 0.132(1+\xi)\eta^2}
\end{aligned}
\tag{25}
$$

F. Direct Method

In this method, mechanical properties of U-D fibre presented in Table 1 are inserted into Eqs. (12), (15), (19) and (23) to obtain properties of bi-axial and tri-axial laminates. Using this approach, significantly higher values for Young's moduli along "1" and "2" directions than experimentally reported values in Table 1 are obtained. This is originated from the fact that the volume fraction of glass fibre in U-D ply is reported as 44%; whereas it is reported as 38% for bi-axial and tri-axial laminates. Therefore, this approach cannot be applicable as the reported experimentally values for U-D ply in Table 1 cannot be extended to the U-D plies in bi-axial and tri-axial fabrics.

G. Inverse Method

In this method, we assume that mechanical properties of U-D fibres in bi-axial and tri-axial laminates are unknown. Thus, considering sets of Eqs. (14), (17), (21) and (25), we have 14 equations with 14 unknown parameters. Namely all Q_{XX}, Q_{XY}, Q_{YY} and Q_{SS}, which are also unknown. It should be noted that in this approach, properties of U-D fabrics (reported in Table 1) are totally different from properties of U-D fabrics constructing bi-axial and tri-axial laminates due to different volume fractions.

At a glance, it can be seen that solving this set of equations due to its non-linear nature is not simple. Since some of these equations are highly dependent on other equations, ordinary and classical solutions are not possible. In order to simplify the solution, it should be known that the major Poisson's ratio of a [0/90] composites has to have an amount between 0.05 and 0.1; this point is chosen as a start point of solution. And by considering β as a known parameter will reduce the number of unknowns. Furthermore, in such situation, there is no need to use complex equations of tri-axial composite with [0/90/-45] configuration. The equations of [0/90/-45] will be used just to verify the results. Using trial and error approach, it was realized that when considering β as a value of 0.06 will result in acceptable values for mechanical properties of U-D fabrics.

According to Table 1, elastic modulus of tri-axial laminates is placed between the upper and lower values. However, using upper and middle values as the first guess in inverse method will not lead to acceptable results; therefore lower magnitude for elastic modulus is the value selected. Now, using obtained results and available equations, E_2 of tri-axial composite with [0/±45] configuration and its Poisson's ratio can be calculated. Therefore, full mechanical properties of bi-axial and tri-axial laminates are extracted. These values are inserted in Table 2.

TABLE 2 CALCULATED MECHANICAL PROPERTIES FOR BI-AXIAL AND TRI-AXIAL LAMINATES

Laminate Name	Configuration	E_1 (GPa)	E_2 (GPa)	ν_{12}	E_6 (GPa)
Bi-axial	[0/90]	16.7*	16.7*	0.06	2.01
Tri-axial	[0/±45]	17.6*	7.01	0.52	5.075

*: experimental observation (See Table 1)

In order to verify the results, elastic modulus of tri-axial composite with [0/90/-45] configuration is also calculated and compared with its original amount which has been obtained from experiment and reported by its supplier [9]. According to aforementioned calculation, amount of this elastic modulus is equal to 13.6 GPa and it is located in the reported interval in Table 1 (15±2.3 GPa). The obtained values in Table 2 (for bi-axial and tri-axial) laminates and experimentally obtained values for U-D fabrics (the first row of Table 1) are used as required mechanical properties in FE model. The lay-up sequence of the both shell and spar structures of the blade are entered into ANSYS very carefully in complete accordance with technical drawings of the blade. A cut section of a real finite element model considering thickness of different parts is depicted in Fig. 5.

The final check is carried out on the whole structure of the blade. The first natural frequencies of the blade associated with flap-wise and edge-wise are obtained using modal analysis of ANSYS and compared with available experimental data [12]. A good agreement between these results is reported in Table 3, which has established our confidence toward proper FE modelling of the blade.

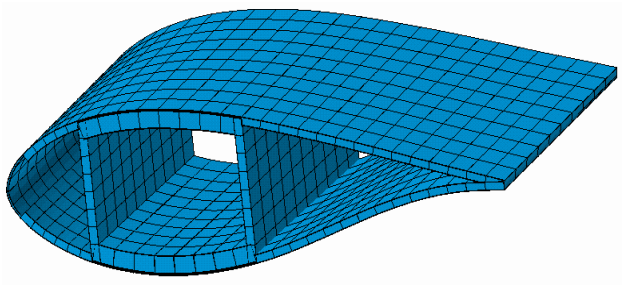

Fig. 5 A cut section of the FE model of the investigated blade

TABLE 3 FREE VIBRATIONS ANALYSIS OF INVESTIGATED WIND TURBINE BLADE

	Flap-wise frequency (Hz)	**Edge-wise frequency (Hz)**
FEA	1.089	1.953
Experimental data [12]	1.09	1.97
Error estimation %	0.09	0.8

V. LOADINGS

A wind turbine blade experiences different load cases during its mission arising from various resources. The load cases are defined as a combination of specific operating and external conditions [13] as illustrated in Fig. 6.

Due to the very rare occurrence of extreme external condition and fault operation conditions and as a result of insignificant influence of the events after the occurrence of the fault and transport, erection and maintenance on aeroelasticity, normal operating conditions and normal external conditions are taken into account in this research chapter.

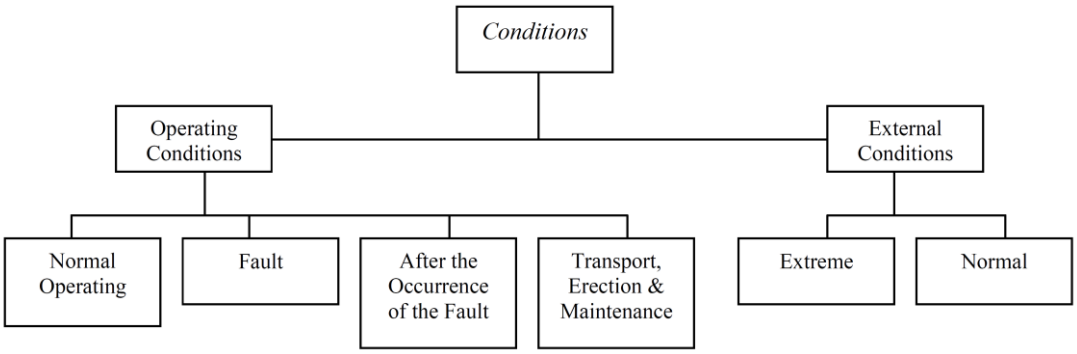

Fig. 6 Operating and external conditions on a wind turbine

Normal operating conditions are divided into four events: (i) stand-by, (ii) start-up, (iii) power production and (iv) normal shut-down events.

(i) Stand-by condition is defined as the situation that there is neither a fault/shut-down condition nor wind speed is outside the range of power production interval.

(ii) Start-up event takes place when the turbine is experiencing transient event either from stand-by to power production situation or from lower wind speed to higher value during power production.

(iii) In power production condition, a turbine generates power within cut-in and cut-out wind speeds.

(iv) Normal shut down implies on transient situation from power production to stand-by conditions or from a higher wind speed to a lower one.

The associated wind speeds with different events of normal operating conditions are presented in Table 4 accompanied with comprising load cases.

Among all load cases, aerodynamic loading on the blade is of a great importance for aeroelasticity analysis. The wind turbine blade is also subjected to other load cases consisting of blade, changes in wind direction, annual gust, centrifugal force, gyroscopic forces due to yaw movements of the turbine, force arisen from start/stop angular acceleration and activation of mechanical brake during different events. The aforementioned load cases were evaluated and it was found out that gyroscopic forces and the force arising from mechanical brake activation can be neglected in comparison with the other load cases. Aerodynamic loading is obtained using aerodynamical FEM which has been already constructed in section III. Germanschier Lloyd rules have provided a clear insight to calculate other mentioned load cases [13].

TABLE 4 CLASSIFICATION OF NORMAL OPERATING CONDITIONS AND INVOLVED LOAD CASES

Wind Speed V (m/s)	$V < 4$	$V = 4$	$4<V<25$	$V = 25$
Event / Load case	**Stand-by**	**Start-up**	**Power production**	**Shut-down**
Aerodynamic load	☑	☑	☑	☑
Weight of blade	☑	☑	☑	☑
Annual gust	☑	☑	☑	☑
Changes in wind direction	☑	☒	☑	☒
Centrifugal force	☒	☒	☑	☒
Gyroscopic forces	☒	☒	☑	☒
Start/stop angular acceleration	☒	☑	☒	☑
Activation of mechanical brake	☒	☒	☒	☑

VI. ANALYSIS OF FLUID-STRUCTURE INTERACTION (FSI)

A comprehensive aeroelastic analysis was performed on normal operating conditions of the turbine covering all stand-by, start-up, power production and shut-down events. For stand-by and start up events, wind speed is assumed equal to 4 m/s according to Table 4. For the event of shut-down, 25 m/s is chosen as the wind flow speed. For the interval of 4 to 25 m/s which is representative of power production event, once 15 m/s is selected as the rated wind speed and also another simulation is carried out on the most frequent wind speed in the mentioned interval. Statistical study on the governing wind pattern of the wind farm provides the probability density function of the wind regime in the form of the Weibull distribution [14]. Weibull function of the wind farm for the investigated turbine was expressed as [15]:

$$h(V) = \left(\frac{1.425}{9.3206}\right)\left(\frac{V}{9.3206}\right)^{(0.425)} e^{-\left(\frac{V}{9.3206}\right)^{1.425}} \tag{26}$$

where, V is a wind speed and $h(V)$ is the corresponding probability of occurrence. The mode wind speed as the most frequent happening wind speed is obtained as 5 m/s. The Weibull graph corresponding to Eq. (26) is drawn in Fig. 7.

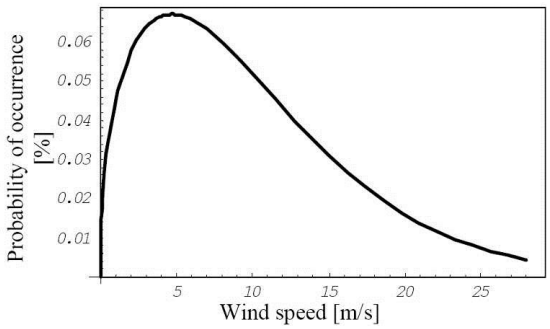

Fig. 7 Probability density function of the wind flow [15]

The global flowchart of semi-couple method for studying the fluid-structure interaction (FSI) of the blade is presented in Fig. 8. In this method an iterative approach is employed to investigate the aeroelastic behaviour of the wind turbine blade. The modelling procedure contains three different phases: aerodynamic analysis, structural analysis and convergence study.

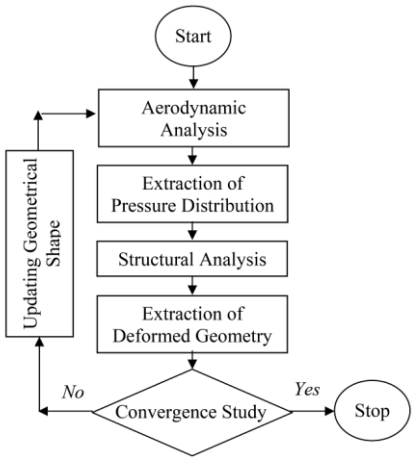

Fig. 8 Flowchart of semi-coupled approach for aeroelasticity study

The modelling starts by an aerodynamic analysis on the primary and undeformed geometry of the blade. The aerodynamic analysis is performed on constructed aerodynamic FE model (section III) using fluid solver of ANSYS software. The output of the aerodynamic analysis which is obtained in the form of pressure distribution on each node is converted to the structural loading for the preceding step of aeroelastic analysis. Obtained aerodynamic loadings and specific combinations of other load cases, summarized in Table 4, are applied to the structural FE model. A non-linear static analysis is executed on structural FE model to obtain deformed shape of the blade. The main reason of conducting non-linear analysis is placed behind the fact that the long and flexible structure of the blade experiences the nonlinearly in the form of large rotation. The deformed shape of the blade is considered as the updated geometrical shape for aerodynamic analysis in the next iteration and the whole procedure is repeated till the convergence is met. The solution is converged when the deflection of the blade experiences stationary status. If the convergence is met, the iteration stops and the final results are reported.

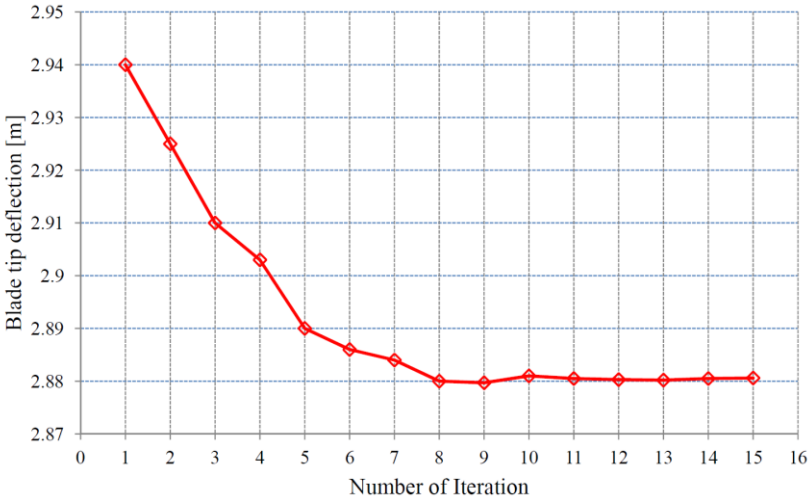

Fig. 9 Convergence of iterative aeroelastic solution

A sample convergence study for iterative aeroelastic simulation is shown in Fig. 9 for the event of power production wherein wind flow speed is taken equal to 5 m/s. It can be seen from Fig. 9 that the solution is converged after eight iterations.

VII. RESULTS AND DISCUSSION

The variation in aerodynamic loading arisen from aeroelasticity phenomenon is reported in Fig. 10 for different events in comparison with corresponding events without aeroelastic coupling consideration. It can be inferred from presented results in Fig. 10 that the most influenced case is attributed to the power production event at rated wind speed which will significantly affect the power production efficiency of the wind turbine. Although the maximum wind speed is used in the aeroelastic simulation for the event of normal shut-down, the variation is less pronounced comparing to power production and start-up. This is originated from the fact that in this event the blade is rotated using pitch mechanism, thus total deflection of the blade will be reduced. So it can be understood that pitch power regulating mechanism does not only regulate the power production of the turbine by adjusting aerodynamic performance of the blade but also has a positive influence on structural behaviour of the blade by exposing stiffer cross sections of the blade to the experienced loadings.

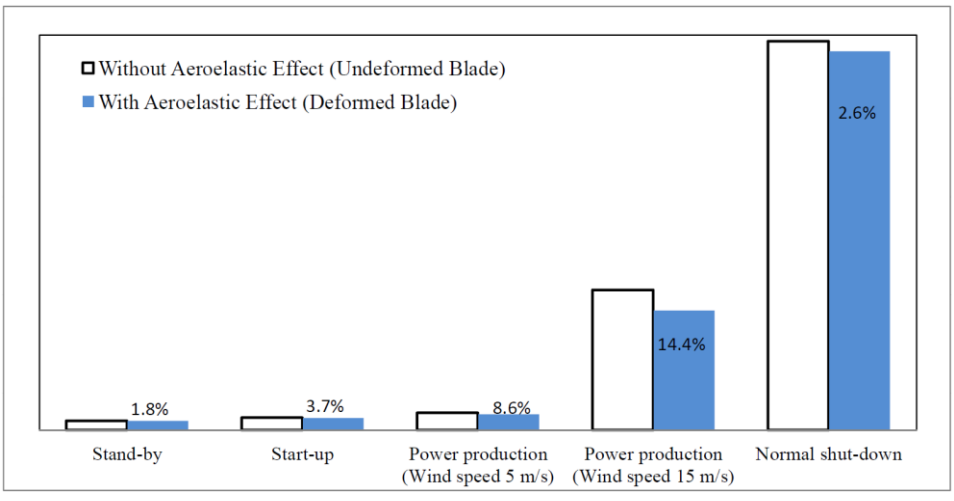

Fig. 10 Variations in aerodynamic loading due to aeroelastic coupling [16]

As a matter of fact, the results imply that the blade deformation has a considerable influence on aerodynamic loadings. For better understanding of this correlation, the distribution of aerodynamic forces along the blade length is presented in Fig. 11 for the event of power production at rated wind power speed (V=15 m/s). The results reveal significant reduction in aerodynamic forces which stems from variations in the effective angle of attack of blade cross sections at different stations.

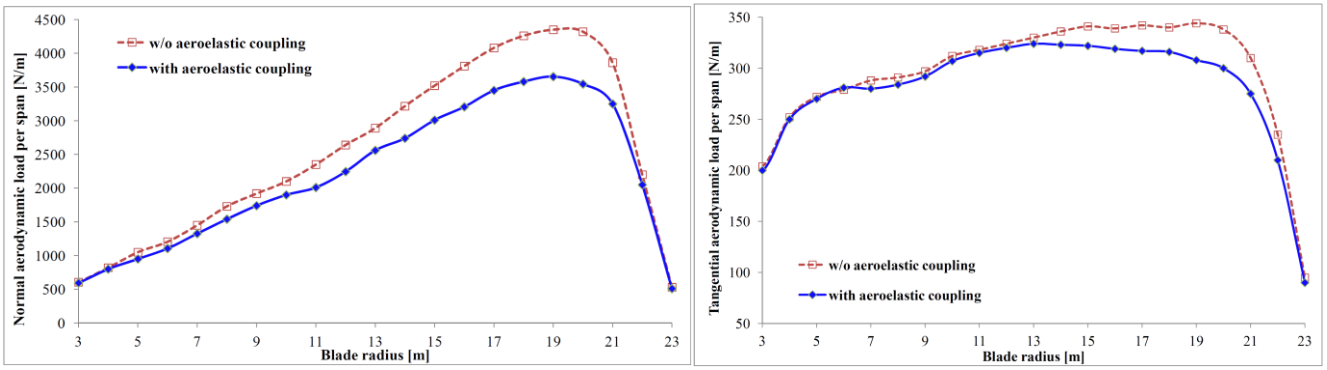

Fig. 11 Distribution of aerodynamic forces at rated wind speed

As a consequence of the variation in aerodynamic loadings, it is expected that induced stress components in critical regions of the blade structure vary too. A comparison between maximum stress components with both aeroelastic coupling and without aeroelastic coupling is presented in Table 5. It is worth mentioning that due to the pitch control system, the location of critical regions wherein maximum stress components are experienced varies for each event in accordance with global status of the blade. Due to unsymmetrical lay-up sequence of composite laminates in the blade structure, it can be seen that induced stress components in some cases are increased.

TABLE 5 MAXIMUM STRESS COMPONENTS AND TIP DEFLECTION OF THE BLADE [16]

Event	Tip Deflection (m)		Longitudinal Stress (MPa)		Transverse Stress (MPa)		In-plane Shear Stress (MPa)	
	A*	B**	A	B	A	B	A	B
Standby	1.22	1.23	503.2	520.1	12.2	13.6	19.7	21.3
Start-up	1.64	1.67	602.4	650.3	9.3	12.9	30.1	32.5
Power production (5 m/s)	2.88	2.94	693.2	705.3	14.6	15.8	28.1	29.2
Power production (15 m/s)	4.07	4.21	762.6	725.0	17.3	15.5	20.4	18.1
Shut-down	4.28	4.33	747.6	764.0	27.41	19.0	17.6	21.3

*A: results with aeroelastic coupling, **B: results without aeroelastic coupling [17]

VIII. CONCLUSIONS

Subjected to different load cases arisen from variety of experiencing events, the blades of modern HAWTs are fully made of composite materials to provide a strong and light structure. The very large and flexible structure of the wind turbine blade necessitates the investigation of aeroelasticity phenomenon for better understanding of the aerodynamic performance of the blade in capturing the wind energy. The interaction between elastic and aerodynamics forces, i.e. static aeroelasticity, is studied for a composite wind turbine blade. A 3D finite element model of the blade is built. A proper aerodynamic model is constructed for extracting aerodynamic forces due to the considerable contribution of this load case in mechanical behaviour of the blade. Another finite element model for application of structural analysis is also built on the same geometry platform of the aerodynamic model while all detailed structural aspects are taken into account. The mechanical properties of all comprising composite laminates are extracted using available limited experimental data and the model is verified to raise the confidence toward employment of proper FE model. In addition to the aerodynamic forces, other load cases, occurred during the normal operating conditions of the blade, are identified and evaluated.

A semi-couple approach is utilized for studying fluid-structural interactions. At the very first stage, the preliminary geometry of the blade (unreformed shape) is analyzed and aerodynamic forces are extracted. All load cases are applied to the structural FE model and non-linear static analysis is carried out to obtain the deflected shape of the blade. The deformed shape of the blade is used to extract updated aerodynamic forces in accordance with updated geometry of the blade and then the results of aerodynamic forces are inserted into structural solver as the input. This approach is repeated until the stationary deflected shape of the blade is obtained. Four different normal operating conditions as stand-by, start-up, power production and normal shut-down are analyzed. For the event of power production, two different wind inflow speed associated with rated wind power and also the mode wind speed value obtained from statistical analysis of governing wind pattern are studied. The results demonstrate that generally efficiency of wind turbine blade is reduced due to the variations imposed to the effective angle of attack along the length of the blade. Since the investigated wind turbine blade is equipped with pitch power regulating mechanism, which can rotate blade along its length with wind inflow speed variation, the total deflection of the blade does not

necessarily increase in higher wind speeds. The results imply on variations of the induced stress levels in critical regions which is important from structural point of view.

REFERENCES

[1] Y. Golfman, *Hybrid Anisotropic Materials for Wind Power Turbine Blades*, CRC Press, Taylor & Francis Group, 2012.

[2] A. Brent Strong, *Fundamental of Composites Manufacturing Material, Methods, and Applications*, 2nd ed., Society of manufacturing engineers, 2008.

[3] D. A. Spera, *Wind Turbine Technology*, ASME Press, New York, 1994.

[4] http://www.vestas.com/.

[5] Ansys Ver 5.4, User Manual, Element Manual, SAS IP Inc., 2003.

[6] "Prepreg technology," Hexcel Composites, Duxford, 1997.

[7] H. J. Sutherland, "On the fatigue analysis of wind turbines," Sandia National Laboratories, Albuquerque, New Mexico, Jun. 1999, SAND99-0089.

[8] J. F. Mandel, D. D. Samborsky, D. S. Cairns, "Fatigue of composite materials and substructures for wind turbine blades," Sandia National Laboratories, Albuquerque, New Mexico, March 2002, SAND2002-0771.

[9] "HexPly Data Sheets, M9.6 Series for Wind Turbine Blade Application, Hexcel Composites Co., 2002.

[10] Data Sheets, M9.6 Series for Wind Turbine Blade Application, Hexcel Composites Co., France Branch, 2002.

[11] S. W. Tsai, S. V. Hoa, D. Gay, Composite Materials, Design and Applications, CRC Press, 2003.

[12] "Technical Description: SSN47-660," Sabaniroo Co., Iran, 200.

[13] Germanischer Lloyd, *Rules and Regulations, IV – Non-Marine Technology*, Regulation for the certification of Wind Energy Conversion System, Germany: Germanischer Lloyd, 1993.

[14] R. Gasch, J. Twele, *Wind Power Plants, Fundamental, Design, Construction & Operation*, James & James, 2002.

[15] M. M. Shokrieh, R. Rafiee *Fatigue life prediction of wind turbine rotor blades manufactured from composites*, In: Vassilopoulos, A. P., Editor, *Fatigue Life Prediction of Composites and Composite Structures*, Woodhead Publishing Limited, Oxford Cambridge New Delhi, 2010.

[16] R. Rafiee, M. Fakoor, "Aeroelastic investigation of a composite wind turbine blade," Wind and Structures, In Press, 2013.

[17] M. M. Shokrieh, R. Rafiee, "Simulation of fatigue failure in a full composite wind turbine blade," Composite Structures, vol. 74, pp. 332-342, 2006.

Dr. Roham RAFIEE has received his PhD in 2010 from mechanical engineering Dept. of Iran University of Science and Technology focusing on nanocomposites. He has done his MSc and BSc theses in the field of composite materials and structures. He has published 20 ISI papers, 30 international conference papers and two chapters of two different books in Woodhead publishing and Springer. He has also registered three patents in the field of nanocomposites and composite structures. He has 11 years of experience in different industrial sections including wind turbines, composite pipes, strategic planning and technology transfer projects. His research interests can be summarized as carbon nanotube reinforced polymers, mechanics of composite materials, design and analysis of composite structures, fatigue modelling of composite structures, finite element modelling and analysis. He is currently an assistant professor of the Faculty of New Sciences and Technologies in University of Tehran. He is already the vice president of a company producing composite pipes and also member of the board of a company producing wind turbines. He is also senior consultant of different companies and industrial group. He is currently cooperating with University of Weimar (Germany) as a member of PhD community and also UPM (Malaysia) as an advisor of PhD thesis.

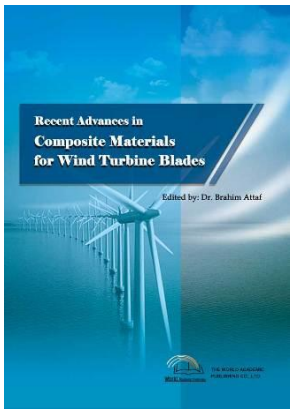

Recent Advances in Composite Materials for Wind Turbine Blades
Edited by Dr. Brahim Attaf

ISBN 978-0-9889190-0-6

Hard cover, 232 pages

Publisher: The World Academic Publishing Co. Ltd.

Published in printed edition: 20, December 2013

Published online: 20, December 2013

This book of science and technology provides an overview of recent research activities on the application of fibre-reinforced composite materials used in wind turbine blades. Great emphasis was given to the work of scientists, researchers and

industrialists who are active in the field and to the latest developments achieved in new materials, manufacturing processes, architectures, aerodynamics, optimum design, testing techniques, etc.. These innovative topics will open up great perspectives for the development of large scale blades for on- and off-shore applications. In addition, the variety of the presented chapters will offer readers access to global studies of research & innovation, technology transfer and dissemination of results and will respond effectively to issues related to improving the energy efficiency strategy for 2020 and the longer term.

How to cite this book chapter

Rafiee R. (2013). On the Fluid-Structure Interaction of a Composite Wind Turbine Blade, *Recent Advances in Composite Materials for Wind Turbines Blades*, Dr. Brahim Attaf (Ed.), ISBN 978-0-9889190-0-6, WAP-AMSA, Available from: http://www.academicpub.org/amsa/chapterInfo.aspx

World Academic Publishing - Advances in Materials Science and Applications